Nanoscale

Accepted Manuscript

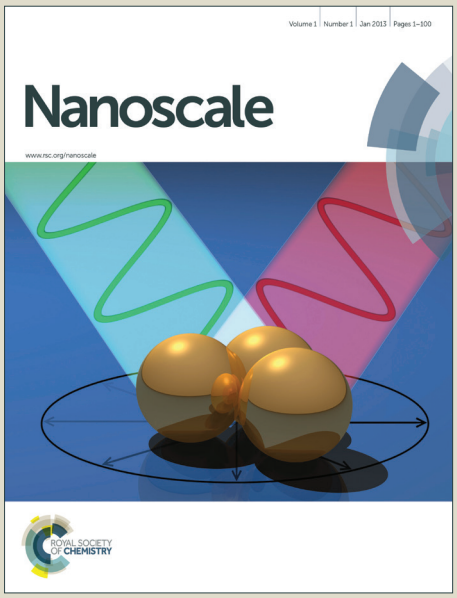

Water flattens graphene wrinkles: laser shock wrapping of graphene onto substrate-supported crystalline plasmonic nanoparticle arrays

Yaowu Hu[1,4+], Seunghyun Lee[3,4,5,6+], Prashant Kumar[1,4,7], Qiong Nian[1,4], Wenqi Wang[1,4], Joseph Irudayaraj[3,5], Gary J. Cheng[1,2,4*]*

[1]School of Industrial Engineering, Purdue University, West Lafayette, Indiana, USA 47907
[2]School of Mechanical Engineering, Purdue University, West Lafayette, Indiana, USA 47907
[3]Department of Agriculture & Biological Engineering, Purdue University, West Lafayette, Indiana, USA 47907
[4]Birck Nanotechnology Centre, Purdue University, West Lafayette, Indiana, USA 47907
[5]Bindley Bioscience Centre, Purdue Center for Cancer Research, Purdue University, West Lafayette, Indiana, USA-47907
[6]Department of Advanced Materials Engineering, University of Suwon, Hwaseong-si, Gyeonggi-do, South Korea 445-743
[7]Department of Physics, Indian Institute of Technology Patna, Patna, India-800013
[+]These authors contributed equally. This work was completed at Purdue University.
[*]Cooresponding authors, email: gjcheng@purdue.edu; josephi@purdue.edu

Abstract:

Hot electron injection into an exceptionally high mobility material can be realized in graphene-plasmonic nanoantenna hybrid nanosystems, which can be exploited for several front-edge applications including photovoltaics, plasmonic waveguiding and molecular sensing at trace level. Wrinkling instabilities of graphene on these plasmonic nanostructures, however, would cause reactive oxygen or sulfur species diffuse and react with the materials, decrease charge transfer rate and block intense hot-spots. No *ex-situ* graphene wrapping technique has been explored so far to control these wrinkles. Here, we present a method to generate seamless integration by using water as a flyer to transfer the laser shock pressure to wrap graphene onto plasmonic nanocrystals. This technique decrease the interfacial gap between graphene and the covered substrate-supported plasmonic nanoparticle arrays, by exploiting a shock pressure generated by laser ablation of graphite and water impermeability nature of graphene. Graphene wrapping of chemically synthesized crystalline gold nanospheres, nanorods and bipyramids with different field confinement capabilities are investigated. A combined experimental and computational method, including SEM and AFM morphological investigation, molecular dynamics simulation, and Raman spectroscopy characterization, is used to demonstrate the effectiveness of this technique. Graphene covered gold bipyramid exhibits the best result among the hybrid nanosystems studied. We have shown that the hybrid system fabricated by laser shock can be used for enhanced molecular sensing. The technique developed has the characteristics of tight integration, chemical/thermal stability, instantaneous, scale and room temperature processing capability, and can be further extended to integrate other 2D material with various 0-3D nanomaterials.

Keywords: Graphene, wrinkle, water, Raman spectroscopy, laser shock wrapping, gold nanoparticle

Introduction

Graphene, a unique ultra-thin, ultra-strong two-dimensional crystal from an earth-abundant element, carbon, features with high carrier mobility, optical transparency, hydrophobicity, chemical inertness and property tunability. The research on graphene has boosted the progress in various disciplines including materials science, electronics, physics, mechanical, bio- and chemical engineering, directly or indirectly within a very brief span of time[1,2]. Graphene-based namomaterials would be the next exciting topic with integrated properties of graphene and functionality of the other components. Plasmonic nanostructures have the capability of collective oscillating free electrons at a metal-dielectric interface under the resonant excitation electromagnetic wave, and have already been demonstrated to significantly enhance performances of nanophotonic devices[3–5], imaging[6], sensing[7,8], energy conversion[9], and material manipulations[10]. Interactions of graphene and plasmonic materials have been under increasing interest in the recent years[11]. Coating of graphene on the surface of these materials could therefore result in a new class of thermally and electrically conducting, optically transperant, chemically inert surfaces and thus one can design hybrid nanomaterials with tunable physical properties with potential to be utilized in a variety of applications. For example, enhanced photoemission from graphene covered ZnO films was observed due to transformation of resonant excitation of graphene plasmon into propagating photons through the interface[12]. Hybrid systems with graphene superimposed over metallic nanostructures were explored to have higher chemical-/bio-sensing capability due to its chemical enhancement effect, chemical protection of metallic surfaces[13–16] and prevention of photocarbonization and photobleaching of target molecules[17,18]. Graphene coating on metallic nanowires was also reported to have increased thermal and electrical conductivity for better thermal management and higher speed in future electronic devices[19].

Strategies for integration of graphene with various nanomaterials include *in-situ* wrapping of graphene while nanostructures are being formed by chemical reactions[20–29] or post-growth *ex-situ* graphene wrapping of nanostructures[30,31]. Ex-situ graphene integration techniques[32–35], such as wet chemical transfer, are the most commonly employed approaches, due to their flexibility of transferring graphene deterministically onto various target surfaces with controlled graphene thickness and integrity. However, such transfer methods are incapable of conformal coating and most often give rise to wrinkles and gaps. It has been noticed that graphene is subject to both intrinsic microscopic corrugations[36] and extrinsic wrinkle instability[37–39]. Periodic ripples of suspended graphene are found to form spontaneously[40] and manipulation of the intrinsic ripple features of graphene is found to effectively influence optical and electronic properties by inducing an effective gauge field[41–44]. For graphene transferred onto a structured surface, the morphology of graphene is influenced by graphene-substrate interaction and it is quite distinct from the random intrinsic wrinkles of free-standing graphene. This extrinsic morphology, also referred to as a snap-through instability of graphene[45,46], is crucial for the fine tuning of physical properties of graphene and more importantly, the graphene-covered systems. Wrinkles and ripples of graphene could drastically influence the chemical activity of the system[47,48], to result in reactive oxygen or sulfur species diffusion or reaction with substrate underneath[49,50], decrease charge transfer rate and block the accessibility of intense hot-spots beneath it.

Graphene wrinkles are solely determined by the elastic properties of graphene, geometrical dimensions of nanoparticles and interfacial adhesion energies. However, this equilibrium nonconformal morphology has large number of bubbles at the interface. There have not yet

been any attempts to seek methods with high efficiency and fidelity to minimize graphene wrinkles.

In this paper, we report a room temperature integration technique, named laser shock wrapping (LSW), which is featured with effective integration, fast processing time and scalability. Water is used to transfer the generated shock pressure to conformally wrap graphene on nanoparticles. To demonstrate its effectiveness, we have examined the surface morphologies at various stages by AFM measurements. Surface-enhanced Raman scattering (SERS)[8], a spectroscopic technique based on Raman scattering and enhancement of molecular signatures of analytes in the "hot spots" of the plasmon field due to metal nanostructures, is employed to investigate the influences of LSW on SERS signatures of molecules in the graphene-plasmonic gold nanoparticle hybrid system.

Results and discussions

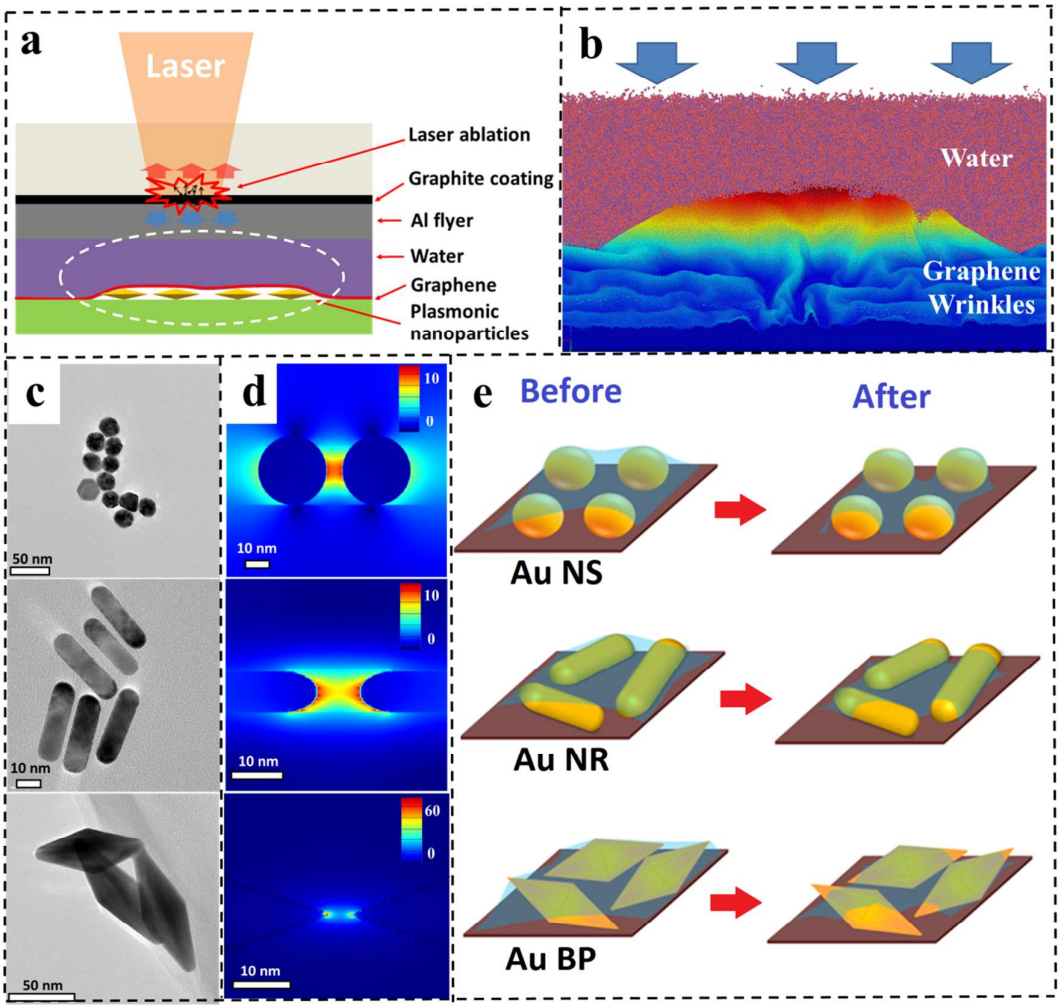

Figure 1. (a) Schematic of the experimental set-up for LSW of graphene. (b) detailed schematic of graphene wrinkles at 3D surfaces and the surrounding water for shock wrapping (area shown in white circle of (a)). (c) TEM images of crystalline nanospheres, nanorods, and bipyramids. (d) FDTD simulation of field confinement of the corresponding nanoparticles in

(c). (e) Schematic drawing of initial graphene wrapping morphologies and laser shock wrapping effect.

Three gold nanostructures with increasing anisotropy, namely gold nanospheres (Au NS), gold nanorods (Au NR)[51] and gold bipyramids (Au BP)[52], as shown in Figure 1 (c) from top to bottom respectively, to investigate the effect of LSW of graphene. Figure S1 shows the absorption spectra for Au NS, Au NR and Au BP. Longitudinal (peak in 520-540 nm range) and transverse (peak centred ~780 nm) plasmonic modes can be observed in the absorption spectra for Au NS, Au NR and Au BP. It should be noted that owing to the symmetric geometry, Au NS shows only transverse plasmonic mode and does not exhibit longitudinal plasmonic mode. While on the other hand, Au NR and Au BP being asymmetric nanostructures, exhibit both transverse as well as longitudinal plasmonic modes.

The schematic shown in Figure 1(a) illustrates the experimental procedure to attain the integration of graphene with plasmonic nanostructures. A shock pressure in MPa magnitude could be effectively generated by using laser abation of sacrificial graphite coating on aluminum foil[53]. Heat transfer from the ablated area is significantly slower and weaker than stress wave propagation. For heat transfer, the characteristic length could be calculated by,

$$l_T = 2\sqrt{\frac{k}{\rho c}t}$$

where k is the thermal conductivity of aluminum; ρ is the density; c is specific heat and t is the time of interest. The characteristic length for stress wave propagation is,

$$l_S = \sqrt{\frac{E}{\rho}t}$$

where E is the young's modulus of aluminum. l_T is calculated to be 140 nm while l_S is 25 µm. Thus the high temperature involved in plasma generation would not affect the underlying graphene-plasmonic hybrid structures. Plasmonic materials, such as silver or even gold, would oxidize or degrade under thermal treatment when exposed to air. Sharp features under heating would undergo shape transformations and thereby would change their functionality. The room temperature processing capability of LSW could thus eliminate such concerns and drive the construction of graphene based multi-material hybrids for potential applications in functional nanostructures and devices.

Figure 1(b) sketches the detailed wrapping mechanism of graphene with external wrinkles when it is placed on non-flat surfaces. Water remains in liquid state at room temperature under the pressure used in current experiment, according to its phase diagram. The interaction of graphene and water has previously been investigated by both molecular dynamics simulations[54–58] and experimental studies[59]. Graphene, despite being one-atom thickness, is found to be impermeable to liquids including water[60,61] and various gases[61,62], resulting from a substantial electron density of its aromatic ring to prevent atoms and molecules from passing through. This characteristic feature of graphene allows us to use water to conformaly shape graphene onto 3D plasmonic nanostructures.

The cold stress shock wave, supported by a fluid with low compressibility and viscosity- i.e. water, could effectively flaten gaps between graphene and the underlying 3D surface, as illustrated in Figure 1 (e). TEM images shown in Figure 1 (c) indicate that the plasmonic nanostructures are crystalline and can withstand high hydrostatic pressure due to the size effect. Representative near fields of these plasmonic nanoparticles under external electromagnetic wave excitation are calculated by using FDTD method, as shown in Figure 1 (d). For nanoparticle arrays supported on a solid substrate, the field enhancements in the gap area between two closely placed nanoparticles are usually much higher than an isolated single

particle, especially for the bipyramid shape. However, these spots are usually difficult to access for graphene due to its in-plane elasticity, which is detrimental to the performance of graphene covered plasmonic nanostructures.

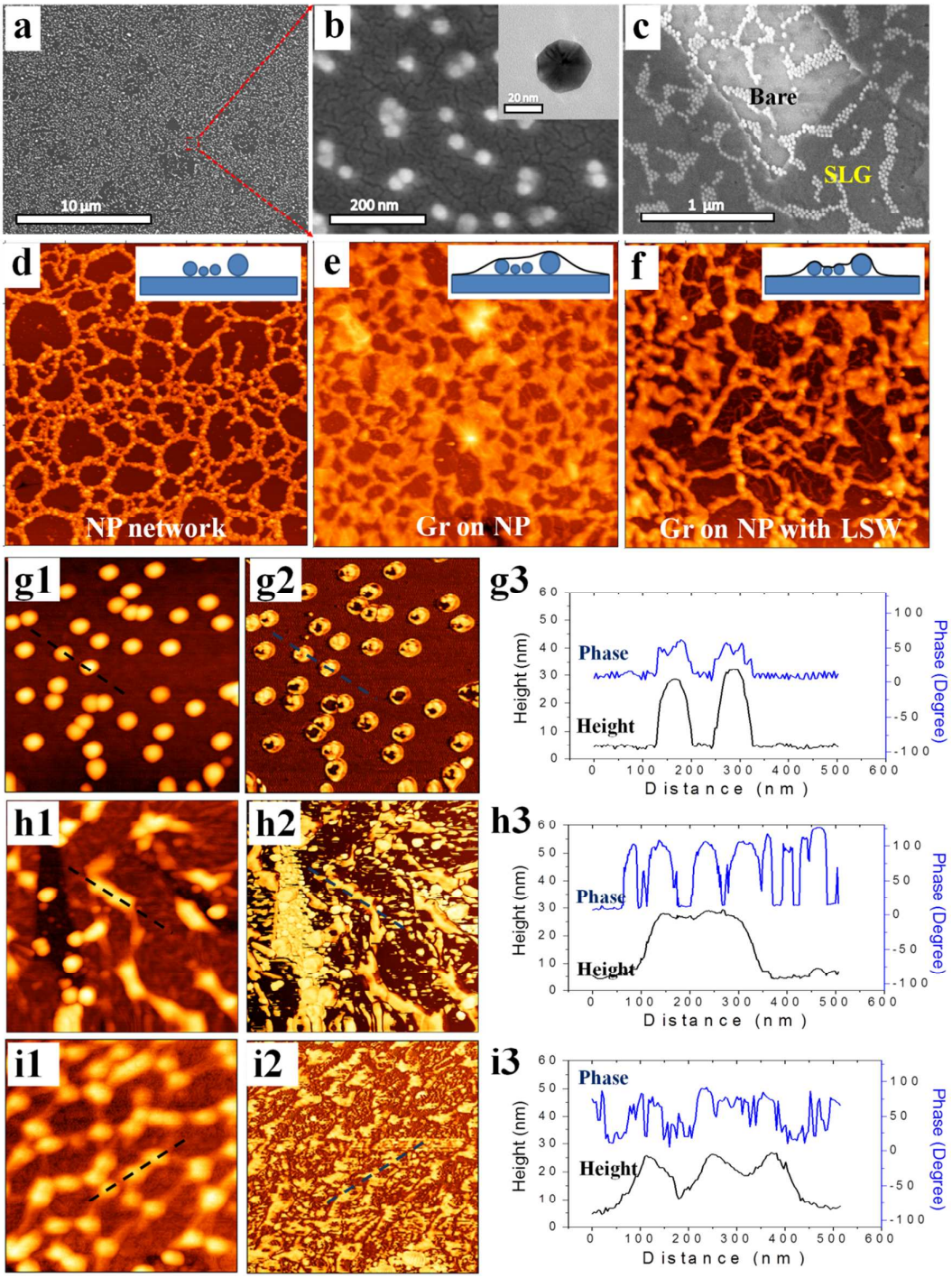

Figure 2. (a) SEM image of nanoparticles on substrate; (b) high resolution SEM image of (a), inset is TEM image of single nanosphere; (c) SEM image of Au nanoparticle networks after graphene transfer; The area without graphene is brighter due to electron charging. (d-f) Large-area AFM images of nanoparticle networks on glass substrate, with single layer graphene transferred on top before and after laser shock integration, respectively. Image sizes

are 10 μm×10 μm. (g-i) AFM images of nanoparticles before graphene transfer, with wet transferred graphene on top and after LSW, respectively. (1-3 are the height image, phase image, and line profiles of heights and phases along the lines shown in 1 and 2, respectively.) Image sizes are 1 μm × 1 μm.

LSW is very effective for graphene covered nanoparticle networks. Figures 2 (a, b) show large-area and high-resolution SEM images of nanoparticles array coated on glass substrates respectively. The high density of the nanoparticles on silicon dioxide substrate would enable tunneling wrinkles and suspended graphene at areas even without any particles underneath, as shown in Figure 2 (c) and (e). Since the nanoparticles are on glass substrates and are very tiny, the effects of LSW are characterized by AFM measurements as shown in Figure 2 (d-f). As the 2D sheets of graphene are transferred onto Au nanoparticle networks, the measured average surface height was found to be significantly increased while the aspect ratio of the resulting nanoshapes was decreased, as shown in Figure S4 in ESI. These are attributed to wrinkles and air voids located at the graphene/nanoparticle assembly interfaces, especially for particles with high density and slightly different particle dimensions. For the just transferred sample, graphene remains suspended in the center of the networks where nanoparticles rarely exist. With LSW, graphene is forced by water pressure to be attached to the substrate in such areas where there is no nanoparticle. Probability plots of height and aspect ratio (H/W) of Au nanoparticles at randomly selected locations shown in Figure S4 in ESI demonstrate the effectiveness of LSW.

Besides the improvement of graphene-substrate interactions, the integration of graphene and plasmonic nanostructures is also greatly enhanced. As shown in Figure 2(h1), after the transfer of graphene, individual nanoparticles are connected by suspended graphene (graphene acting like a hood to these nanoparticles). When atomic force microscopy is carried out, some nanoparticles are inaccessible to the AFM tip due to carbon atoms in graphene. It should be kept in mind that graphene sheet lies on nanoparticles due to mechanical strength. Figure 2(h2) represents phase angle variation of oscillating AFM tip during its interaction with surfaces with inhomogeneous mechanical properties. A higher phase angle indicates locally stiffer sample surface. Comparison of height and phase information at the same locations are shown in Figure 2(h3). At places with suspended graphene, phase angle drops dramatically due to decreased stiffness. The phase angle variation is around 100 degree for wet-transferred samples. Measured height reductions at the center of adjacent nanoparticles are ~2 nm. With the help of LSW, phase variation drops to ~50 degree, which is the typical value of the original sample without graphene covering. Height variation between adjacent nanoparticles is~15 nm, indicating that graphene wrinkles have been minimized. Gap areas between two particles are quite distinguishable, in samples which have undergone LSW as shown in Figure 2(i1).

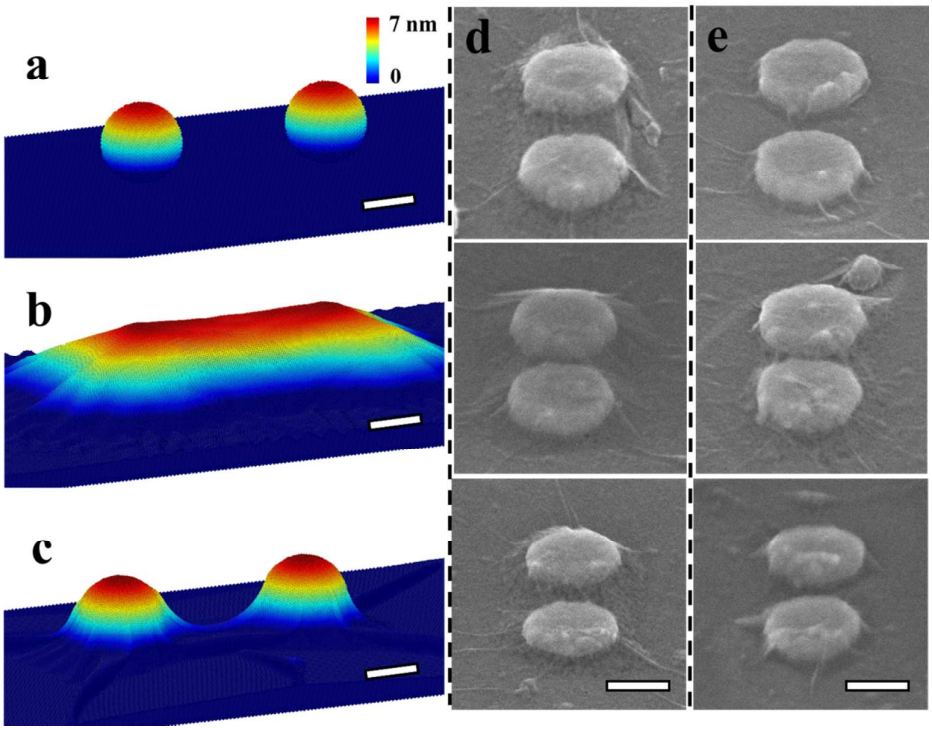

Figure 3. (a-c) Molecular dynamics simulations of nanoparticles on substrate, graphene wrinkles after wet transfer, and laser shock wrapped graphene, respectively. Scale bars: 5 nm. Tilted SEM (45^0) imaging of graphene wrinkles on plasmonic nanostructures before (d) and after LSW (e). Scare bars: 200 nm.

Two nanoparticles with 8 nm diameter and 12 nm gap are used in the molecular dynamics simulation. Graphene bridges the two particles at the initial equilibrium, as shown in Figures 3(b) and (d). The formation of such wrinkles has already been discussed in the literature[37]. With LSW, graphene in the center region could be attached to the middle ground due to graphene sliding, elastic straining[63], and strain energy release during graphene crack propagation, as shown in Figure 3(c) and (e). The simulated results in Figures 3(a-c) agree qualitatively well with the experimental results in Figure 2 and Figure 3. It can be seen that the wrinkling instability of graphene, which depends on competing effects of the surface adhesion energy and graphene's conformal elastic strain energy could be changed by LSW and replaced with another equilibrium states with better conformability.

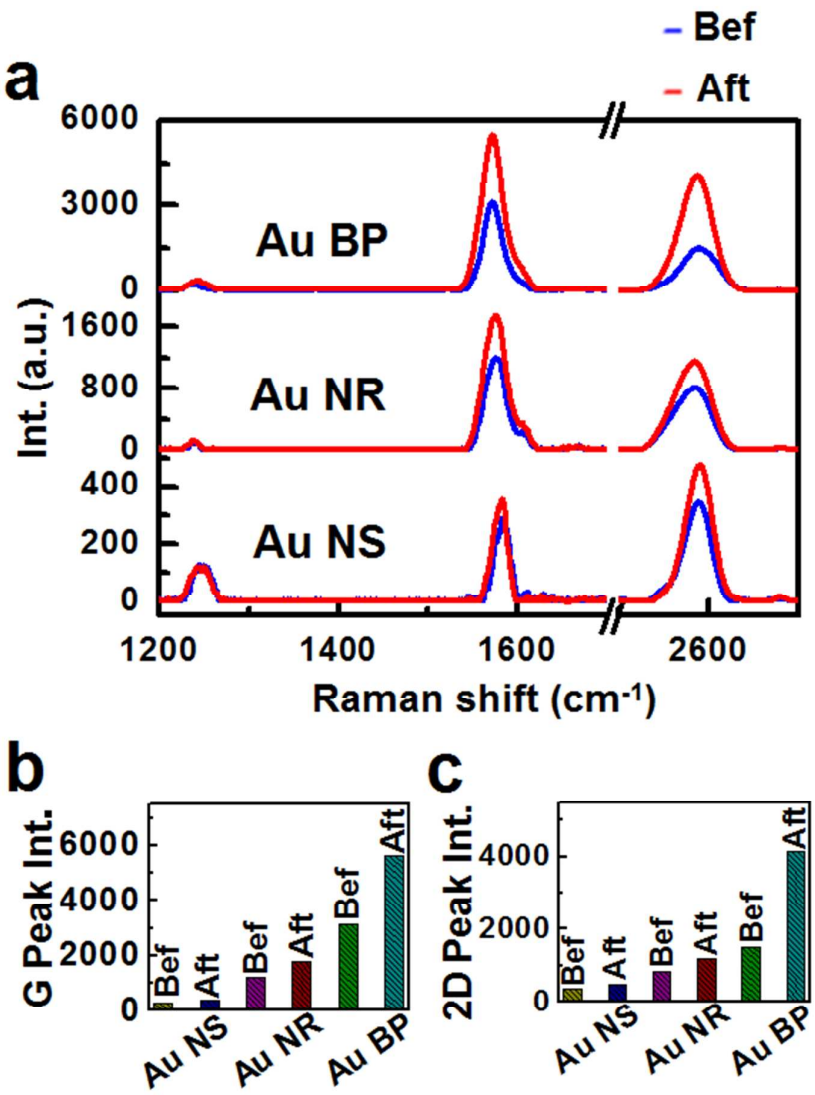

Figure 4. (a) Raman spectra of graphene on Au NS, Au NR and Au BP before and after LSW. Plot depicting (b) G and (c) 2D peak intensity of various samples before and after laser shock.

Raman spectroscopy experiments of graphene, as transferred and laser shock integrated with plasmonic nanostructures, would establish the impact of laser shock on the quality of interface. On the other hand, graphene, being a macromolecule; would show whether the localized plasmon in such plasmonic nanostructures would enhance the characteristic Raman signals of graphene. To support our claim, an enhancement in Raman 2D and G peak for all the three types of samples namely Au NS, Au NR and Au BP was noted and shown in Figure 4(a). Raman intensities for G and 2D peaks were separately plotted for different samples and shown in Figure 4(b) and (c). Graphene could hardly be excited by 785 nm infrared laser due to insufficient photon energy to excite the vibrational modes. However, when graphene is supported by the plasmonic nanoparticles, fluorescence background of the substrate is quenched while the normal weak Raman signitures of graphene are enhanced, as shown in Figure 4. A further enhancement of 2D and G intensities after LSW proves that graphene is pushed to tiny gaps areas with highly enhanced local fields. Due to charge doping of Au nanoparticles and lowered mirror symmetry of valence and conduction bands in wrapping, the 2D/G intensity ratios of monolayer graphene are found to have lower values than those

reported[64] where graphene is situated on a dielectric substrate. This effect is more evident in the case of graphene on nanorods and bipyramids since they are more asymmetrical than nanospheres. The small splitting of the G band of graphene when placed on Au nanorods demonstrates a slightly broken phonon symmetry near the Γ point. While for graphene placed on Au bipyramids and nanospheres, the symmetry of CC double stretching is found to be preserved. The D peaks for all samples before and after LSW are low, indicating a high integrity of graphene initially and minimal damage induced by LSW. The highest D peak intensity is found on the nanosphere samples, despite its highest symmetry among the three, indicating that the predominant factor in introducing defects is the size of the nanoparticle, other than the aspect ratios or asymmetrical levels. With larger particle size, graphene might break due to excessive local straining effect (see Figure 3(e)).

Au BP shows the maximum enhancement among the tested geometries. Compared to the more symmetric Au nanoparticles such as nanospheres and nanorods, the effect of LSW is more obvious for anisotropic Au BP. Such an enhancement upon laser shock is expected, as the corners and facets in the BP sample as well as the gaps between two or more BP nanoparticles are more unlikely to be accessed by graphene. These areas of BP have its highest field confinement in the nanoparticles considered (Figure 1 (d)). Intensity of 2D peak of graphene increased more than twice for graphene with LSW, compared with that for graphene merely wet-transferred. The two-fold overall enhancement results from a 800-fold local enhancement was achieved (assuming one 10 nm× 10 nm gap area in every 200 nm × 200 nm sample area). Such a noticeable Raman enhancement upon laser shock processing provides exciting evidence of improved interfaces between graphene and gold nanostructures. Statistic analysis of Raman spectra at a variety of locations shows that the G peaks of graphene on Au BP, exhibit smaller fluctuations compared to the same sample before LSW. Slight shifts in 2D and G Raman fingerprints of graphene are observed after LSW, due to combined influences of local 3D straining and charge transfer under Raman laser excitation.

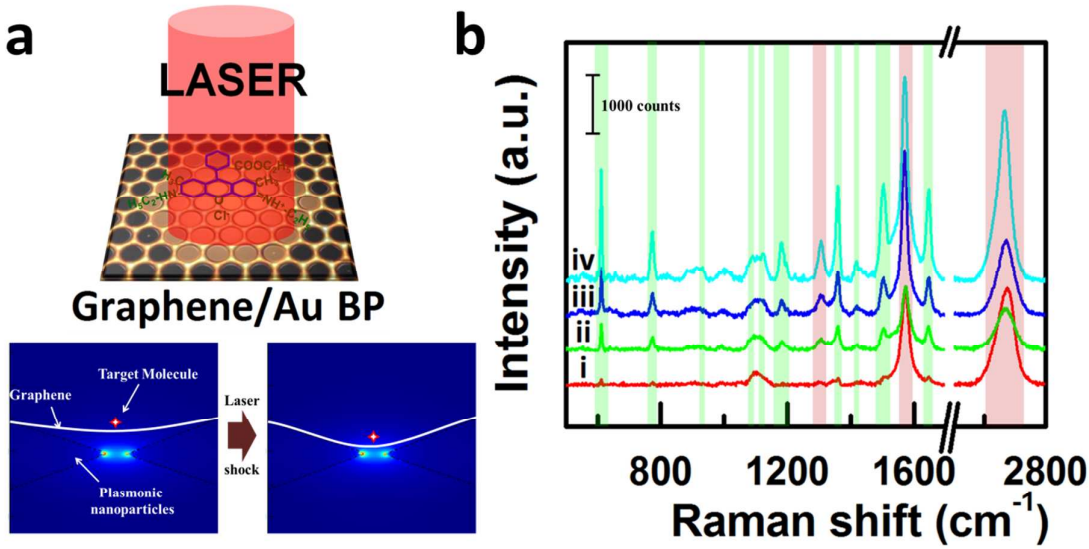

Figure 5. (a) Schematic for label-free molecular detection, (b) SERS spectra of R6G on graphene transferred on Au BPs before LSW and at 1 nM concentration (i) and the same after LSW for (ii) 1 nM, (iii) 500 nM and (iv) 5 μM concentrations of R6G. Raman peaks marked with red shade represent 2D, G and D Raman signatures of graphene and those marked with green shade represent peaks from R6G.

After achieving a significant Raman enhancement in graphene, due to the localized plasmonic field; further applications can be pursued. R6G molecules were coated on graphene wrapped Au BP to test the molecular sensing capability. The characteristic Raman peaks of the R6G molecules which were almost absent for the 1 nM concentration of graphene transferred on the Au BP (see Figure 5(b)(i)), appears after laser shock processing in a significant manner, as shown in Figure 5(b)(ii). Figure 5(b)(iii) and (iv) shows the Raman signal for 500 nM and 5 μM of R6G. The Raman peak positions for R6G molecule (614, 776, 933, 1088, 1127, 1181, 1360, 1420, 1506, and 1648 cm^{-1}) were in close agreement with the literature[65,66]. Graphene covered plasmonic nanostructure hybrid systems have been found to result in higher molecular sensing capabilities. However, in many cases as graphene wrinkles on these 3D nanostructures, molecules are blocked from reaching areas with high local fields, and thus the benefits of graphene are compromised. In the present study, as the hidden hot spot appears, both graphene and target molecules could be excited by localized surface plasmon, which contributes to enhanced sensitivity. Interactions of molecules and the anchoring surface would however, marginally shift Raman peaks. It should be noted that by adjusting the laser power, density of Au BP used and further optimizing nanoparticle shapes, detection in lower concentrations such as pM or fM range could be achieved.

In conclusion, LSW, a laser shock induced effective integration of graphene with plasmonic nanostructures has been demonstrated. The technique utilizes the shock pressure generated by laser ablation and water impermeability of graphene to effectively flatten graphene wrinkles on 3D surfaces. Observed enhancement of 2D Raman fingerprints of graphene facilitated by the enormous localized plasmonic field due to the facile integration of materials achieved by laser shock pressure was validated. Laser shock integrated graphene-plasmonic hybrid nanosystems have further been explored for label-free molecular detection via Raman spectroscopy. We have shown that 1nM of R6G molecules anchored on graphene laser shocked onto Au BP exhibit Raman peaks which are clearly distinguishable. It should be noted that the laser shock integration technique is scalable, instantaneous in nature and possesses room temperature capability. The laser shock integration technique is not limited to graphene-plasmonic nanostructures system, and can further be extended to other 2D materials with various target nanostructures including photonic crystals and quantum dots.

Methods

Laser Shock wrapping (LSW): Single layer graphene (SLG) coated on copper sheet by chemical vapour deposition (CVD) were commercially obtained. The top surface is then spin coated with PMMA (approximately 100 nm thin) at 3000 rpm and cured at 180 ^{0}C for 2 minutes. The underlying copper substrate was then wet-etched away employing $FeCl_3$ aqueous solution. PMMA/graphene stack was then completely washed with DI water several times and transferred on top of the Au nanogeometries such as nanospheres, nanorods and bipyramids. After adequate drying, the sample is then soaked in acetone for 30 minutes to dissolve PMMA and cleaned with Isopropyl Alcohol (IPA) and further dried. Laser shock wrapping of SLG with that of gold nanoparticles is carried out to reduce the gap between them. As shown in Figure 1(a), a Q-switch Nd-YAG laser (Continuum Surelite III) with 5 ns pulse duration is used to provide the energy source for laser shock wrapping. Various laser intensities have been tested for the purpose and an optimized laser intensity of 0.05 GW/cm^2 was employed for all the sample preparation to enable wrapping but avoid flattening of nanoparticles[67]. Aerosol graphite painting (Asbury Carbons, U.S.A.) coated on 4 μm

aluminum film (Lebow Company Inc., Bellevue, WA) absorbs the laser energy, gets vaporized and ionized to provide ultrahigh shock pressure in the downward direction. A water layer is placed below the aluminum foil and above the graphene layer to transfer the shock pressure and enable conformal wrapping effect. A motorized XYZ stage is employed to conveniently adjust the laser processing area.

Characterization: SEM imaging was carried out with a Hitachi S-4800 field-emission scanning electron microscope. Veeco Dimension 3100 atomic force microscope was employed for acquiring AFM images and line profiles which were used for statistical analysis of aspect ratio. Transmission electron microscope (FEI Tecnai) was employed for achieving electron images of single gold nanoparticle. UV-VIS-NIR spectrometer (Scinco) was used to measure the plasmon bands of the gold nanoparticles. Raman spectrometer (Bruker Senterra) equipped with near-infrared laser (λ = 785 nm) was used for acquiring Raman signatures of graphene on plasmonic gold nanoparticles.

MD simulations: Molecular dynamics modeling was performed to illustrate initial graphene wrinkling morphology on nanoparticle arrays and laser shock wrapping effect. The gold nanoparticle dimer is with 8 nm diameter and 12 nm gap and FCC structure. Adaptive intermolecular reactive empirical bond order (AIREBO) potential was used for graphene. The cutoff distance is 2.0Å. Graphene with free ends is of size 160 nm$\times$50 nm.Gold-graphene interactions were modeled by a Lennard Jones (LJ) potential $V(r) = 4\ \varepsilon_{c\text{-}Au}\ (\sigma_{c\text{-}Au}^{12}/r^{12} - \sigma_{c\text{-}Au}^{6}/r^{6})$, where $\varepsilon_{c\text{-}Au}$ = 0.01273 eV, $\sigma_{c\text{-}Au}$= 2.994 Å.[68–70] The vdW interaction between graphene and the substrate is modeled by using the same potential with parameters $\varepsilon_{c\text{-}Au}$ = 0.00891 eV, $\sigma_{c\text{-}Au}$= 3.629 Å.[71] The system is calcualted in ensemble NVT (Nose-Hoover thermostat) with the temperature maintained at 300 K. The time step is 1 fs.

Acknowledgements

The authors gratefully acknowledge funding from the National Science Foundation (Award# 0809463, 1233783, 1249315), National Institute of Health (Award# CA157395-01), Purdue Research Foundation Incentive Grant, Indiana next generation manufacturing competitiveness center (IN-MaC), and the Center for Food Safety Engineering (USDA-ARS-Purdue University) grant.

Received: ((will be filled in by the editorial staff))
Revised: ((will be filled in by the editorial staff))
Published online: ((will be filled in by the editorial staff))

References

1 A. K. Geim and K. S. Novoselov, *Nat. Mater.*, 2007, **6**, 183–191.

2 K. S. Novoselov, a K. Geim, S. V Morozov, D. Jiang, M. I. Katsnelson, I. V Grigorieva, S. V Dubonos and a a Firsov, *Nature*, 2005, **438**, 197–200.

3 S. Lal, S. Link and N. J. Halas, *Nat. Photonics*, 2007, **1**, 641–648.

4 W. Barnes, A. Dereux and T. Ebbesen, *Nature*, 2003, **424**, 824–830.

5 E. Ozbay, *Science*, 2006, **311**, 189–93.

6 X. Zhang and Z. Liu, *Nat. Mater.*, 2008, **7**, 435–441.

7 M. E. Stewart, C. R. Anderton, L. B. Thompson, J. Maria, S. K. Gray, J. a Rogers and R. G. Nuzzo, *Chem. Rev.*, 2008, **108**, 494–521.

8 K. Lee and J. Irudayaraj, *J. Phys. Chem. C*, 2009, **113**, 5980–5983.

9 S. Linic, P. Christopher and D. B. Ingram, *Nat. Mater.*, 2011, **10**, 911–21.

10 M. L. Juan, M. Righini and R. Quidant, *Nat. Photonics*, 2011, **5**, 349–356.

11 Q. Mu, G. Jiang, L. Chen, H. Zhou, D. Fourches, A. Tropsha and B. Yan, *Chem. Rev.*, 2014, **114**, 7740–7781.

12 S. W. Hwang, D. H. Shin, C. O. Kim, S. H. Hong, M. C. Kim, J. Kim, K. Y. Lim, S. Kim, S. H. Choi, K. J. Ahn, G. Kim, S. H. Sim and B. H. Hong, *Phys. Rev. Lett.*, 2010, **105**, 1–4.

13 C. Guo, B. Book-Newell and J. Irudayaraj, *Chem. Commun.*, 2011, **47**, 12658.

14 D. Prasai, J. C. Tuberquia, R. R. Harl, G. K. Jennings and K. I. Bolotin, *ACS Nano*, 2012, **6**, 1102–1108.

15 P. M. Wilson, A. Zobel, A. Lipatov, E. Schubert, T. Hofmann and A. Sinitskii, *ACS Appl. Mater. Interfaces*, 2015, **7**, 2987–2992.

16 Y. Su, V. G. Kravets, S. L. Wong, J. Waters, a. K. Geim and R. R. Nair, *Nat. Commun.*, 2014, **5**, 4843.

17 P. Wang, O. Liang, W. Zhang, T. Schroeder and Y.-H. Xie, *Adv. Mater.*, 2013, **25**, 4918–24.

18 W. Xu, X. Ling, J. Xiao, M. S. Dresselhaus, J. Kong, H. Xu, Z. Liu and J. Zhang, *Proc. Natl. Acad. Sci. U. S. A.*, 2012, **109**, 9281–6.

19 R. Mehta, S. Chugh and Z. Chen, *Nano Lett.*, 2015, 150206084313000.

20 J. S. Lee, K. H. You and C. B. Park, *Adv. Mater.*, 2012, **24**, 1084–8.

21 D. Wei, J. Liang, Y. Zhu, Z. Yuan, N. Li and Y. Qian, *Part. Part. Syst. Charact.*, 2013, **30**, 143–147.

22 Y. Chen, F. Guo, A. Jachak, S.-P. Kim, D. Datta, J. Liu, I. Kulaots, C. Vaslet, H. D. Jang, J. Huang, A. Kane, V. B. Shenoy and R. H. Hurt, *Nano Lett.*, 2012, **12**, 1996–2002.

23 J. Luo, X. Zhao, J. Wu, H. D. Jang, H. H. Kung and J. Huang, *J. Phys. Chem. Lett.*, 2012, **3**, 1824–1829.

24 Y. Xu, R. Yi, B. Yuan and X. Wu, *J. Phys. Chem. Lett.*, 2012, **3**, 309–314.

25 R. Ma, Z. Lu, C. Wang, H.-E. Wang, S. Yang, L. Xi and J. C. Y. Chung, *Nanoscale*, 2013, **5**, 6338–43.

26 S. S. Jyothirmayee Aravind and S. Ramaprabhu, *J. Appl. Phys.*, 2012, **112**, 124304.

27 H. Wang, Y. Yang, Y. Liang, J. T. Robinson, Y. Li and A. Jackson, 2011, 2644–2647.

28 K.-S. Ahn, S.-W. Seo, J.-H. Park, B.-K. Min and W.-S. Jung, *Bull. Korean Chem. Soc.*, 2011, **32**, 1579–1582.

29 Y. Shi, S.-L. Chou, J.-Z. Wang, D. Wexler, H.-J. Li, H.-K. Liu and Y. Wu, *J. Mater. Chem.*, 2012, **22**, 16465.

30 H. Y. Song, S. F. Geng, M. R. An and X. W. Zha, *J. Appl. Phys.*, 2013, **113**.

31 Y. F. Li, H. Q. Yu, H. Li, C. G. An, K. Zhang, K. M. Liew and X. F. Liu, *J. Phys. Chem. C*, 2011, **115**, 6229–6234.

32 X. Li, Y. Zhu, W. Cai, M. Borysiak, B. Han, D. Chen, R. D. Piner, L. Colombo and R. S. Ruoff, *Nano Lett.*, 2009, **9**, 4359–63.

33 X. Liang, B. a Sperling, I. Calizo, G. Cheng, C. A. Hacker, Q. Zhang, Y. Obeng, K. Yan, H. Peng, Q. Li, X. Zhu, H. Yuan, A. R. H. Walker, Z. Liu, L.-M. Peng and C. a Richter, *ACS Nano*, 2011, **5**, 9144–53.

34 J. W. Suk, A. Kitt, C. W. Magnuson, Y. Hao, S. Ahmed, J. An, A. K. Swan, B. B. Goldberg and R. S. Ruoff, *ACS Nano*, 2011, **5**, 6916–24.

35 D.-Y. Wang, I.-S. Huang, P.-H. Ho, S.-S. Li, Y.-C. Yeh, D.-W. Wang, W.-L. Chen, Y.-Y. Lee, Y.-M. Chang, C.-C. Chen, C.-T. Liang and C.-W. Chen, *Adv. Mater.*, 2013, **25**, 4521–6.

36 J. C. Meyer, a K. Geim, M. I. Katsnelson, K. S. Novoselov, T. J. Booth and S. Roth, *Nature*, 2007, **446**, 60–63.

37 S. Zhu and T. Li, *J. Appl. Mech.*, 2014, **81**, 061008.

38 Y. Zhou, Y. Chen, B. Liu, Z. Yang, M. Hu and S. Wang, *Carbon N. Y.*, 2014, **84**, 263–271.

39 T. Li, *Model. Simul. Mater. Sci. Eng.*, 2011, **19**, 054005.

40 W. Bao, F. Miao, Z. Chen, H. Zhang, W. Jang, C. Dames and C. N. Lau, *Nat. Nanotechnol.*, 2009, **4**, 562–6.

41 F. Guinea, M. I. Katsnelson and M. a H. Vozmediano, *Phys. Rev. B - Condens. Matter Mater. Phys.*, 2008, **77**, 1–8.

42 F. Guinea, B. Horovitz and P. Le Doussal, *Phys. Rev. B - Condens. Matter Mater. Phys.*, 2008, **77**, 1–8.

43 a. L. Vázquez De Parga, F. Calleja, B. Borca, M. C. G. Passeggi, J. J. Hinarejos, F. Guinea and R. Miranda, *Phys. Rev. Lett.*, 2008, **100**, 1–4.

44 N. N. Klimov, S. Jung, S. Zhu, T. Li, C. a. Wright, S. D. Solares, D. B. Newell, N. B. Zhitenev and J. a. Stroscio, *Science (80-.).*, 2012, **336**, 1557–1561.

45 S. Scharfenberg, N. Mansukhani, C. Chialvo, R. L. Weaver and N. Mason, *Appl. Phys. Lett.*, 2012, **100**, 2010–2013.

46 T. J. W. Wagner and D. Vella, *Appl. Phys. Lett.*, 2012, **100**.

47 D. W. Boukhvalov and M. I. Katsnelson, *J. Phys. Chem. C*, 2009, **113**, 14176–14178.

48 A. Politano and G. Chiarello, *Carbon N. Y.*, 2013, **61**, 412–417.

49 A. Kimouche, O. Renault, S. Samaddar, C. Winkelmann, H. Courtois, O. Fruchart and J. Coraux, *Carbon N. Y.*, 2014, **68**, 73–79.

50 Y. Zhang, Q. Fu, Y. Cui, R. Mu, L. Jin and X. Bao, *Phys. Chem. Chem. Phys.*, 2013, **15**, 19042–8.

51 C. Yu and J. Irudayaraj, *Anal. Chem.*, 2007, **79**, 572–579.

52 S. Lee, K. Mayer and J. Hafner, *Anal. Chem.*, 2009, **81**, 4450–4455.

53 H. Gao, Y. Hu, Y. Xuan, J. Li, Y. Yang, R. V. Martinez, C. Li, J. Luo, M. Qi and G. J. Cheng, *Science (80-.).*, 2014, **346**, 1352–1356.

54 T. a. Ho and A. Striolo, *J. Chem. Phys.*, 2013, **138**.

55 J. Rafiee, X. Mi, H. Gullapalli, A. V Thomas, F. Yavari, Y. Shi, P. M. Ajayan and N. a Koratkar, *Nat. Mater.*, 2012, **11**, 217–22.

56 T. Werder, J. H. Walther, R. L. Jaffe, T. Halicioglu, P. Koumoutsakos, M. Field, E. Corporation, W. F. a V and V. Sunny, *J. Phys. Chem. B*, 2003, **107**, 1345–1352.

57 Q. Li, J. Song, F. Besenbacher and M. Dong, *Acc. Chem. Res.*, 2015, **48**, 119–127.

58 P. Cao, K. Xu, J. O. Varghese and J. R. Heath, 2011, 5581–5586.

59 J. Zang, S. Ryu, N. Pugno, Q. Wang, Q. Tu, M. J. Buehler and X. Zhao, *Nat. Mater.*, 2013, **12**, 321–5.

60 R. R. Nair, H. A. Wu, P. N. Jayaram, I. V. Grigorieva and A. K. Geim, *Science (80-.).*, 2012, 335, 442–444.

61 J. S. Bunch, S. S. Verbridge, J. S. Alden, A. M. Van Der Zande, J. M. Parpia, H. G. Craighead and P. L. McEuen, *Nano Lett.*, 2008, **8**, 2458–2462.

62 D. Jiang, V. R. Cooper and S. Dai, *Nano Lett.*, 2009, **9**, 4019–4024.

63 J. Li, T.-F. Chung, Y. P. Chen and G. J. Cheng, *Nano Lett.*, 2012, **12**, 4577–83.

64 a. C. Ferrari, J. C. Meyer, V. Scardaci, C. Casiraghi, M. Lazzeri, F. Mauri, S. Piscanec, D. Jiang, K. S. Novoselov, S. Roth and a. K. Geim, *Phys. Rev. Lett.*, 2006, **97**, 187401.

65 T. T. B. Quyen, C.-C. Chang, W.-N. Su, Y.-H. Uen, C.-J. Pan, J.-Y. Liu, J. Rick, K.-Y. Lin and B.-J. Hwang, *J. Mater. Chem. B*, 2014, **2**, 629.

66 X. N. He, Y. Gao, M. Mahjouri-Samani, P. N. Black, J. Allen, M. Mitchell, W. Xiong, Y. S. Zhou, L. Jiang and Y. F. Lu, *Nanotechnology*, 2012, **23**, 205702.

67 P. Kumar, J. Li, Q. Nian, Y. Hu and G. J. Cheng, *Nanoscale*, 2013.

68 S. Arcidiacono, J. H. Walther, D. Poulikakos, D. Passerone and P. Koumoutsakos, *Phys. Rev. Lett.*, 2005, **94**, 3–6.

69 W. Luedtke and U. Landman, *Phys. Rev. Lett.*, 1999, 3835–3838.

70 S.-K. Chien, Y.-T. Yang and C.-K. Chen, *Nanoscale*, 2011, **3**, 4307.

71 B. Qiu and X. Ruan, *Appl. Phys. Lett.*, 2012, **100**.